Iron phthalocyanine in non-aqueous medium forming layer-by-layer films: growth mechanism, molecular architecture and applications†

Priscila Alessio,[abc] Maria Luz Rodríguez-Méndez,[b] Jose Antonio De Saja Saez[c] and Carlos José Leopoldo Constantino*[a]

Received 23rd October 2009, Accepted 20th January 2010
First published as an Advance Article on the web 2nd March 2010
DOI: 10.1039/b922242c

The application of organic thin films as transducer elements in electronic devices has been widely exploited, with the electrostatic layer-by-layer (LbL) technique being one of the most powerful tools to produce such films. The conventional LbL method, however, is restricted in many cases to water soluble compounds. Here, an alternative way to produce LbL films containing iron phthalocyanine (FePc) in non-aqueous media (chloroform) is presented. This film fabrication was made possible by exploiting the specific interactions between Fe and NH_2 groups from PAH, poly(allylamine hydrochloride) used as the supporting layer, leading to the formation of bilayers structured as $(PAH/FePc)_n$. We have also incorporated silver nanoparticles (AgNPs) in LbL films with $(PAH/FePc/AgNP)_n$ trilayers, making it possible to achieve the surface-enhanced Raman scattering (SERS) phenomenon. The molecular architecture of the LbL films was determined through different techniques. The growth was monitored with UV-Vis absorption spectroscopy, their morphology characterized by optical and scanning electron (SEM) microscopes, and their molecular organization determined using FTIR. The electrochemical properties of the LbL films were successfully applied in detecting dopamine in KCl aqueous solutions at different concentrations using cyclic voltammetry. The results confirmed that the LbL films from FePc in non-aqueous media keep their electroactivity, while showing an interesting electrocatalytic effect. The SERS phenomenon suggested that FePc aggregates might be directly involved in the maintenance of the electroactivity of the LbL films.

Introduction

The method of preparing alternating layers was initially proposed by Iler[1] in 1966 for positively and negatively charged colloidal particles. Two decades later, Netzer and Sagiv[2] developed an approach to build up multilayers based on self-association and self-organization through chemical interactions, generally covalent bonds. In the early 1990s, Decher *et al.*[3] reported the preparation of multilayer films through the self-assembly process with the alternating adsorption of anionic and cationic polyelectrolytes on charged surfaces, which was extended in Rubner's group by Ferreira *et al.*[4] for conjugated polyions and by Cheung *et al.*[5] for conducting polymers. The now referred to as the layer-by-layer (LbL) technique has been applied for a wide range of systems including different classes of materials.[6–13] The vast majority of such LbL films are based on electrostatic interactions involving ionic species in aqueous media, which implies restrictions to the materials that can be studied. This is the case of phthalocyanines, for which the LbL technique is basically applied to functionalized molecules that are soluble in aqueous media. For instance, despite all the metallic phthalocyanines (MPc's) available, the most common found forming LbL films are substituted FePc,[14–17] NiPc,[13,17,18] CuPc,[19–21] and CoPc.[22] Recently, Yang *et al.*[23] reported the use of LbL technique to produce films of cationic cobalt tetraaminophthalocyanine (CoTAPc) and anionic tungstophosphate anions (P_2W_{18}) in DMF media. However, the film growth was still based on electrostatic interactions.

Phthalocyanines were discovered in 1907 but their chemical structure was determined only in 1936 by Linstead. They are formed by four isoindol units connected to each other by nitrogen atoms. The substitution of central hydrogen atoms by a metallic atom leads to the MPc's as shown in Fig. 1 for FePc. Among the diverse characteristics of the MPc's, the high thermal and chemical stability are highlighted.[24] In addition, the highly conjugated electronic structure with 18 π electrons combined to properties such as electroactivity, semiconductivity, photoconductivity, photochemical activity, electrochromism, luminescence, non-linear optics, and optical storage lead to great potentiality for diverse applications.[25–32] Particularly important is the possibility of forming thin films of phthalocyanines through different techniques such as LbL,[16,19] physical vapor deposition (PVD) either by thermal evaporation[33,34] or sputtering,[35] Langmuir–Blodgett (LB),[36,37] electrodeposition,[38] spin-coating,[39] and casting,[40]

[a] *Departamento de Física, Química e Biologia, Faculdade de Ciências e Tecnologia, UNESP, SP, 19060-900 Presidente Prudente, Brazil. E-mail: case@fct.unesp.br; Tel: +55 18 3229-5355*
[b] *Inorganic Chemistry Department, E. T. S. Ingenieros Industriales, University of Valladolid, 47011 Valladolid, Spain*
[c] *Condensed Matter Physics Department, Faculty of Science, University of Valladolid, 47011 Valladolid, Spain*
† Electronic supplementary information (ESI) available: Resonance Raman spectra; cyclic voltammograms. See DOI: 10.1039/b922242c

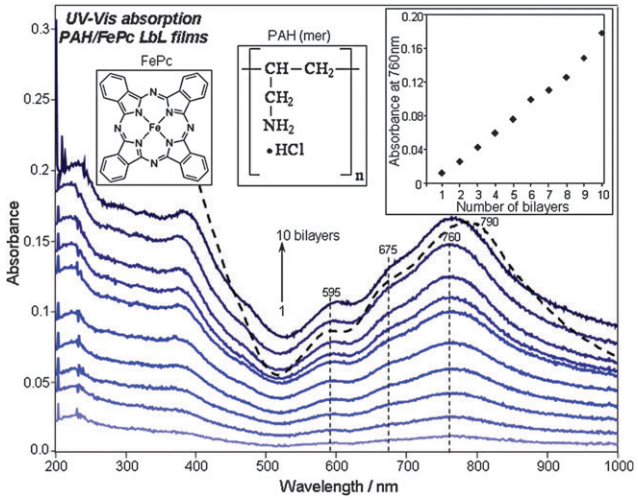

Fig. 1 UV-Vis absorption spectra for LbL films of PAH/FePc containing different numbers of bilayers. The dashed line (---) is the UV-Vis absorption spectrum of the FePc solution in chloroform. The insets show the molecular structures of PAH (mer unit) and FePc and the linear dependence of the absorbance at 760 nm as a function of PAH/FePc deposited bilayers.

since many organic devices use the element transducers in the form of thin films. For instance, promising technological applications have been suggested for phthalocyanines in the form of thin films for light emitting diodes,[41] transistors,[42] solar cells,[19] liquid crystals,[43] fuel cells,[44] and sensors.[45,46] In the case of FePc specifically, we have shown recently its ability to form thin films through LB, PVD, and LbL methods.[15] However, for producing the LbL films a tetrasulfonated iron phthalocyanine (FeTsPc) was required since FePc is water insoluble.

In the present work, a step forward is taken with the LbL technique being used to produce thin films of FePc in non-aqueous medium. The LbL films were grown as bilayers of $(PAH/FePc)_n$ and trilayers of $(PAH/FePc/AgNP)_n$; where PAH is poly(allylamine hydrochloride) and AgNPs are silver nanoparticles. The molecular architecture of the LbL films was investigated through ultraviolet-visible (UV-Vis) absorption spectroscopy (growth monitoring), Fourier transform infrared (FTIR) absorption spectroscopy (molecular organization and growth mechanism), scanning electron microscopy (SEM-morphology), and micro-Raman technique (morphology and growth mechanism). In addition to combining morphological and chemical information by coupling an optical microscope to a Raman spectrograph, we could achieve the surface-enhanced phenomenon for the LbL films containing AgNPs. Finally, the electrochemical activity of phthalocyanines was tested for the LbL films containing FePc using cyclic voltammetry. The sensing capabilities and the electrocatalytic effect were evaluated by analyzing the electrochemical response of the LbL films toward different concentrations of the neurotransmitter dopamine in aqueous solutions.

Experimental methods

Fabrication of LbL films

The $(PAH/FePc)_n$ LbL films were grown from 0.5 mg mL^{-1} of PAH (Aldrich) in aqueous solution prepared with ultrapure water (18.2 MΩ cm) from a Milli-Q system model Simplicity and 0.5 mg mL^{-1} of FePc (Aldrich) in chloroform ($CHCl_3$). In addition, $(PAH/FePc/AgNP)_n$ LbL films were fabricated using Ag colloidal solution obtained by reducing silver nitrate with sodium citrate following the method proposed by Lee and Meisel[47] in 1982 and used as synthesized. The sodium citrate ($C_6H_5Na_3O_7{\cdot}2H_2O$ and MW = 294.1 g mol^{-1}) and the silver nitrate ($AgNO_3$ and MW = 169.88 g mol^{-1}) were bought from Sigma-Aldrich. Basically, the Ag colloid is prepared by dissolving 90 mg of silver nitrate in 500 mL of ultrapure water and heated until boiling. Then the solution is stirred and 10 mL of an aqueous solution of sodium citrate at 1% w/v (for instance, 0.1 g of sodium citrate in 10 mL of ultrapure water) is added by dropping. The solution is kept boiling and stirred for 1 h. The final concentration of the Ag colloid is *ca.* 1.0×10^{-3} mol L^{-1}. Following this method it is expected that the colloidal Ag nanoparticles are negatively charged with a zeta potential of *ca.* −45 mV at pH 5.6 (ultrapure water),[48] present preferentially spherical shape (different structures such as rods, prisms, hexagonal plates and some aggregates are also found) with a size distribution in diameter ranging from 25 to 130 nm with a maximum distribution between 30 and 40 nm.[49–52]

The multilayer LbL films were made by immersing the substrate for 3 min alternately into PAH and FePc solutions in the case of bilayers and PAH, FePc, and Ag colloidal solutions in the case of trilayers. After each deposition step, the films were rinsed with ultrapure water and left drying in air for another 3 min. The speed of withdrawal of the substrates was controlled to be 8.5 mm min^{-1} using a mechanical dipper. The number of bilayers (or trilayers) and the substrate for each film differed depending on the characterization methods. It is important to note that less than 3 min is already enough to reach the equilibrium in terms of forming a FePc layer. We have observed that the main factor that affects this equilibrium is the speed of the substrate when it is removed from the FePc solution. The faster evaporation of the chloroform when compared to the water (usually used in the LbL technique) might be in the origin of this effect. Films with 10 bilayers (PAH/FePc) and 7 trilayers (PAH/FePc/AgNP) were grown onto quartz for UV-Vis absorption spectroscopy while 10 bilayers and 10 trilayers were deposited onto a glass substrate for SEM microscopy. In the latter, the glass substrates were thermally treated at 600 °C for 2 h to minimize their roughness, which was found below 10 Å. The cyclic voltammetry experiments were carried for LbL film with 5 bilayers of PAH/FePc and 5 trilayers of PAH/FePc/AgNP onto indium-tin-oxide (ITO) substrates (ITO and LbL films with 5 bilayers of PAH/FeTsPc fabricated in aqueous media were applied as references). The reason why different numbers of layers were used for characterizing the LbL films with distinct techniques was to match with the sensitivity of these techniques. All the substrates were previously cleaned using neutral detergent being extensively washed with distilled water, then acetone (10 min sonication), chloroform (10 min sonication), and ultrapure water. This procedure was already sufficient to activate the substrate surfaces for the adsorption of the PAH layer avoiding using any other drastic treatments, such as piranha solution (a mixture of concentrated sulfuric acid and

hydrogen peroxide). It is important to comment that it is also possible to grow the LbL film of FePc itself by dipping and drying steps without using PAH. However, the preliminary results that we have obtained point to a lower quality of these FePc/FePc LbL films in terms of molecular architecture.

LbL film characterization methods

The UV-Vis absorption spectroscopy was carried out using a spectrophotometer Varian model Cary 50. The Raman spectra were obtained with both 514.5 and 633 nm laser lines using a spectrograph Renishaw model in-Via, which is coupled to a Leica optical microscope allowing recording spectra point-by-point with a spatial resolution of *ca.* 1 μm^2 using an objective of 50× magnification, and equipped with a CCD detector and 1800 grooves/mm diffraction grating yielding a spectral resolution of *ca.* 4 cm^{-1}. The Raman images were obtained by collecting the spectra along an area or line previously chosen using a *XYZ* motorized stage. The SEM images were recorded using a FEI microscope, model Quanta 200F, under low vacuum (1.0 Torr) and without metalizing the LbL film surfaces. Cyclic voltammetry was carried out using an EG&G PARC 263A potentiostat/galvanostat (M270 Software) with a conventional three-electrode cell. The reference electrode was a saturated Ag|AgCl/KCl electrode and the counter electrode was a platinum plate. The LbL films were immersed into 0.1 M KCl aqueous solution with the dopamine (Aldrich) being added at several steps leading to concentrations at 2.0×10^{-6}, 3.0×10^{-6}, 6.0×10^{-6}, 1.0×10^{-5}, 1.5×10^{-5}, 2.5×10^{-5}, 7.5×10^{-5}, 9.2×10^{-5}, 1.08×10^{-4}, 1.25×10^{-4}, 1.75×10^{-4} and 2.75×10^{-4} M. The cyclic voltammograms were recorded from −1.0 up to +1.0 V at a scan rate of 100 mV s^{-1}, and starting at 0.0 V.

Results and discussion

LbL film growth monitoring—UV-Vis absorption spectroscopy

The growth of the LbL film was monitored with UV-Vis absorption spectroscopy, whose spectra are shown in Fig. 1 for $(PAH/FePc)_n$. The molecular structures of FePc and PAH and the UV-Vis absorption spectrum of FePc in chloroform solution (dashed line) are also displayed. LbL films of PAH/FePc up to 10 bilayers were fabricated and a linear growth of the absorbance with the deposited layers is observed, as indicated in the inset in Fig. 1 for the absorbance at 760 nm *vs.* the number of deposited bilayers. This shows that a similar amount of material is transferred onto the substrate per deposited layer ensuring a uniform growth of the LbL films. The features observed in the UV-Vis absorption spectra are assigned to FePc since PAH does not absorb within this wavelength range. The characteristic B band at shorter wavelengths and Q band at longer wavelengths, which are attributed to the electronic transitions HOMO → LUMO (π electrons), can be clearly seen.[24]

The successful growth of LbL films containing FePc from non-aqueous medium allowed us to take a step forward by growing PAH/FePc LbL films containing AgNPs on top of the FePc layers, thus producing LbL films with trilayers structured as $(PAH/FePc/AgNP)_n$. Fig. 2 shows the UV-Vis absorption spectra up to 7 trilayers, which are basically composed by a superposition of both FePc and AgNP UV-Vis spectra. This is strong evidence that the AgNPs do not interact strongly with PAH/FePc layers, which is desirable since the AgNPs are incorporated aiming at the surface-enhanced Raman phenomena.[53,54] Furthermore, the insets (A) and (B) in Fig. 2 indicate a linear growth of the absorbance *vs.* the number of deposited layers for the bands at 410 nm (assigned to AgNPs) and 760 nm (assigned to FePc) confirming that both materials are adsorbed in a uniform, reproducible way forming trilayer LbL films. Indeed, in the case of the band at 410 nm, a linear regime starts at the 3rd bilayer. The superposition of both AgNP and FePc UV-Vis absorption spectra makes difficult a detailed discussion. However, it could be mentioned that the adsorption of the AgNPs in a different way before and after the 3rd trilayer might be related to the better covered of the substrate. This effect was reported by Goulet *et al.*[55] using atomic force microscopy (AFM) images when growing LbL films of dendrimers/AgNP. Because the substrate is not fully covered for the first 2 bilayers, it plays a different role before and after the 3rd bilayer. The same trend observed for the band at *ca.* 410 nm in the LbL film of PAH/FePc/AgNP was also observed by Goulet *et al.*[55] and Aoki *et al.*[56] (LbL films of PAH/phospholipids containing AgNPs).

The inset (C) in Fig. 2 uses the UV-Vis absorption spectra for both Ag colloid and FePc in chloroform solution as references. In the case of Ag colloid, the strong absorption band with a maximum at 410 nm is assigned to the surface plasmon of isolated AgNPs while the tail that extends to longer wavelengths is attributed to the surface plasmon of AgNP aggregates.[57] The LbL films containing bi- or trilayers were characterized through micro-Raman spectroscopy. The arrows drawn in Fig. 2 at 514.5 and 633 nm indicate the lasers used in the characterization with the Raman technique. The laser line at 514.5 nm is out-of-resonance with FePc, leading the conventional Raman scattering (RS), while the laser line at 633 nm is absorbed by the FePc, which allows recording of the resonance Raman scattering (RRS) spectra whose cross section can be improved until it is 10^6 that of RS.[58] Besides, both laser lines are absorbed by the AgNPs, which is a necessary condition to achieve both surface-enhanced Raman scattering (SERS) and surface-enhanced resonance Raman scattering (SERRS).[53,54]

A complementary discussion considering the UV-Vis absorption spectra can be made regarding phthalocyanine aggregates. Usually, when there is a superposition of two absorption bands in the wavelength range assigned to the Q band in the UV-Vis spectrum, the band at shorter wavelength is assigned to dimers or longer orders of aggregates, while the band at higher wavelength is attributed to monomers.[24,59,60] In our case, Fig. 1 and 2 show a third maximum in the UV-Vis absorption spectra of FePc either in the LbL films or in the solution (Q band). The difference in energy between these maxima (within tenths of eV) suggests transitions from the fundamental to different vibrational energy levels of the first electronic excited state.

This trend was also observed for the same FePc in LB and PVD films.[15] The monomers might be present in the LbL

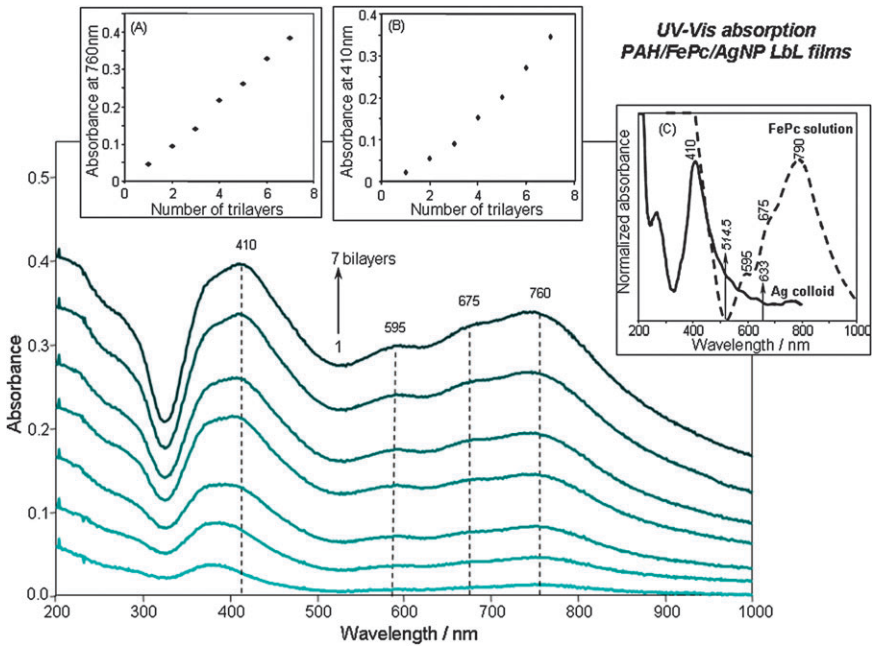

Fig. 2 UV-Vis absorption spectra for LbL films of PAH/FePc/AgNP containing different numbers of trilayers. The insets show the linear dependence of the absorbance at (A) 760 nm and (B) 410 nm as a function of PAH/FePc/AgNP deposited trilayers and (C) the UV-Vis absorption spectra for FePc solution in chloroform and for Ag colloid.

films, however, the formation of aggregates is clearly seen in the optical and SEM images discussed further in Fig. 5 and 6. In fact, the tendency of phthalocyanine aggregating itself either through π–π interactions or bridged by O_2 molecules is reported in the literature.[24,59,61–63] In the case of ref. 62 and 64, LbL films of Pc/Pc grown under certain experimental conditions using the dip and dry process are reported taking advantage of the self-attraction between the Pc molecules. Also worth mentioning is the shift in the UV-Vis absorption band maximum from 790 nm for FePc in solution to 760 nm in the LbL film (either bi or trilayers). This could be related to the formation of FePc aggregates and/or PAH-FePc interactions when forming the LbL films. The latter seems to be a stronger factor, since the aggregates might be already present in the FePc solution. The concentration used here, which is similar to those found in ref. 59, 61 and 62, and the width of the UV-Vis absorption bands, which is practically the same for solution and LbL films[60] as shown in Fig. 1, indicate the presence of FePc aggregates in the solution.

LbL film growth mechanism—SERS and SERRS

The LbL technique was initially conceived for the fabrication of multilayers based on the electrostatic interactions of oppositely charged polyelectrolytes,[3] but it is now known that other types of interaction can also be exploited. For the LbL films produced here with FePc in a non-aqueous medium, the electrostatic interactions between charged groups should not be the dominant mechanism, in contrast to the PAH/FeTsPc LbL films of ref. 16. As we shall show, there is evidence that the interaction between the unprotonated amine donor groups of PAH (NH_2) and the coordinating metal of the phthalocyanine (Fe) is the most important process. In a subsidiary experiment, we failed to produce LbL films from PAH and $LuPc_2$ owing to the lack of interaction with Lu.

The interaction between PAH and FePc is clearly observed in the Raman spectra in Fig. 3 recorded with the 633 nm laser line for the FePc powder (RRS) and LbL films containing 2 bilayers of PAH/FePc (RRS). The assignments for the main FePc Raman bands are given in Table 1 based on ref. 16, 65 and 66. The RRS spectra for the powder and PAH/FePc LbL film differ in terms of the relative intensities for certain bands. In addition, bands that are present in one spectrum are absent in the other and vice-versa. From the assignments in Table 1, several of these bands are directly related to changes in the electronic surrounding of the Fe atom coordinated with the macrocycle ring. This is the case of the bands at 945, 1017, 1180, 1339, 1403, 1519 and 1528 cm^{-1}. This is evidence that not only a chemical interaction involving PAH and FePc is established, which allows the growth of the bilayer LbL films (as suggested previously in the UV-Vis data), but also that this interaction might take place between NH_2 and Fe. This interaction will be confirmed further on with the FTIR data. It is worth mentioning that the differences between the RRS spectra of PAH/FePc and FePc powder are much larger than those reported for LbL films of PAH/FeTsPc grown in aqueous media,[16] which is in full agreement with the strong interaction between PAH and FePc to form LbL films when using non-aqueous medium. One could speculate that such differences in the RRS spectra are due to possible differences in the FePc molecular organization. However, this can be discarded since the Raman spectra recorded for FePc in the form of powder or forming distinct thin films such as LB and PVD present a similar profile (Figure not shown). The powder is found to have a random molecular organization while the FePc molecules are well organized in LB and PVD films,

though with distinct types of arrangement for each film.[15] Another doubt that could be raised at this point is if the PAH is indeed present in the PAH/FePc LbL films. The importance of the PAH in the quality of the PAH/FePc LbL films was mentioned in the Experimental section. Besides, two indirect evidences of the presence of the PAH in the LbL films of PAH/FePc are given in Fig. 1 and 2 of the ESI:† (i) the Raman spectrum for a FePc/FePc LbL film, which was grown by dipping and drying steps, is found to be very similar to the FePc powder and pretty different from the PAH/FePc LbL film (Fig. 1 in the ESI†); (ii) the signals of cyclic voltammetry observed for PAH/FePc and FePc/FePc either in KCl or in dopamine are different for both LbL films (Fig. 2†). Besides, the PAH/FePc LbL film presented a stronger signal for dopamine under the same experimental conditions. The differences mentioned above either for Raman or cyclic voltammetry comparing FePc/FePc and PAH/FePc must be undoubtedly related to the presence of PAH in the LbL film.

In the case of SERRS, depending on the spot of the film, distinct spectra are recorded. However, all of them, in a general way, can be classified in two classes of SERRS spectra. It is shown in Fig. 3 one constituent of each class for the LbL film containing 2 trilayers of PAH/FePc/AgNP. These different spectra are not found in the case of collecting RRS at different spots of the LbL film containing 2 bilayers of PAH/FePc. Therefore, the differences presented by SERRS spectra from spot to spot of the LbL film must depend on the dominant chemical species (FePc aggregates or FePc-PAH linked molecules or a combination of both) that is closer to the AgNPs reached by the incident laser. For instance, one of the SERRS spectrum (A) recorded for the trilayer LbL film presents a profile much closer to the RRS spectrum of the FePc powder. The reason why this SERRS spectrum for the film is similar to the RRS spectrum of FePc powder is because the AgNPs that are adsorbed preferentially onto the layer containing FePc aggregates. Since SERRS is highly distance dependent,[53,67,68] the SERRS spectrum preserves the characteristic vibrational modes of FePc placed at the top of the aggregates (the SERRS signal decreases for angstroms of distance between the target molecules and metal nanoparticles). This also confirms that the interaction between AgNPs and FePc in terms of forming a complex is very weak, which is consistent with the UV-Vis data in Fig. 2, and with the absence of significant interaction between AgNPs and FePc in LB films (Figure not shown) or dip-coated films.[69] On the other hand, the SERRS spectrum (B) in Fig. 3 with the most distinct profile in relation to FePc powder suggests that this kind of spectrum is collected from regions where the FePc-PAH linked molecules might be the dominant chemical

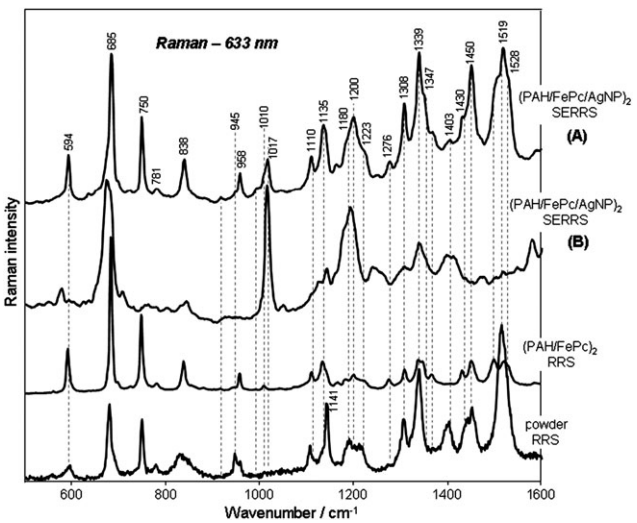

Fig. 3 Raman spectra recorded with the 633 nm laser line for FePc powder (RRS) and LbL films containing 2 bilayers of PAH/FePc (RRS) and 2 trilayers of PAH/FePc/AgNP (SERRS). (A) and (B) refer to SERRS spectra collected at different regions of the LbL films.

Table 1 Raman band center (cm^{-1}) and assignments for FePc (powder and LbL films)

FePc Raman scattering—633 nm laser line			
Powder	PAH/FePc	PAH/FePc/AgNP	Assignments
594	594	594	Macrocycle vibration,[16] ring breathing, N–Fe stretching, benzene expending[65]
685	685	685	Macrocycle vibration,[16] C–N–C N–Fe stretching, pyrrole, expending,[63] benzene deformation[63]
750	750	750	Macrocycle vibration,[16] C–H out-of-plane bending[65]
781	781	781	Isoindole N–Fe stretching
838	838	838	Pyrrole N–Fe stretching, benzene expending, C–N–C in-plane bending[65]
945			N–Fe C–N–C in-plane bending, isoindole deformation[6]
958	958	958	Benzene breathing,[16] C–H out-of-plane bending[6]
1010	1010	1010	C–H in-plane bending,[65,66] benzene expending[65]
1017	1017	1017	N–Fe in-plane bending, ring stretching, benzene deformation[65]
1110	1110	1110	C–H in-plane bending,[65,66] isoindole N–Fe stretching[65]
1135–1141	1135–1141	1135–1141	C–H in-plane bending[16,65]
1180	1180	1180	C–H in-plane bending, pyrrole N–Fe stretching[65]
1200–1223	1200–1223	1200–1223	C–H N–Fe in-plane bending, C–N–C stretching[65]
1276	1276	1276	C–H in-plane bending[6,16]
1308	1308	1308	Isoindole N–Fe stretching, C–H in-plane bending[65,66]
1339	1339	1339	Pyrrole stretching,[16,66] isoindole N–Fe stretching, C–H C–N–C in-plane bending[65]
1403		1403	Isoindole stretching,[16] C–N–C stretching, pyrrole expanding, C–H in-plane bending[65]
1430	1430	1430	Isoindole stretching,[16] C–H in-plane bending, C–C stretching[65]
1450	1450	1450	Isoindole stretching,[16,66] ring stretching, pyrrole N–Fe C–H in-plane bending[65]
1519	1519	1519	C=C, C=N pyrrole stretching,[16] C–N–C stretching, pyrrole expanding, C–H in-plane bending[62]
1528	1528	1528	C–N–C stretching, pyrrole expanding,[65,66] C–H in-plane bending[65]

species closer to the AgNPs reached by the incident laser. The AgNPs could also attach to the surface of PAH that is uncovered by FePc. However, no spectrum is collected in this case because PAH does not present a SERS signal.

With AgNPs mainly physisorbed onto the FePc layer, one should expect enhanced SERS and SERRS signals due to the electromagnetic field enhancement on the AgNP surfaces.[53,54,67] Indeed, Fig. 4 shows that the SERS spectrum for 1 trilayer of PAH/FePc/AgNP is much more intense than the Raman spectrum for 10 bilayers of PAH/FePc in LbL films, with the 514.5 nm laser line under the same experimental conditions. For the same *Y* axis scale, the Raman spectrum (RS) is almost a horizontal line in comparison to SERS. As discussed for SERRS, the SERS spectra also present differences from spot to spot of the LbL film. However, when the RS and SERS spectra collected with the same experimental conditions are plotted in the same *Y* scale, the trend is the same, shown in Fig. 4 (RS is basically a horizontal line). This fact prompts one to estimate the enhancement factor involved in this process. One way to do that is to consider the intensity ratio between two bands that belong to SERS and RS spectra. For instance, the intensity of the strongest SERS band at 1450 cm^{-1} is *ca.* 77 000 photons s^{-1} while in the RS the band at 1450 cm^{-1} is indeed a shoulder whose intensity is *ca.* 70 photons s^{-1} (the intensity is considered as the height from the top to the bottom of the band). Considering the intensity ratio SERS/RS for this band, *i.e.* $\left(\frac{77\,000}{70} \cong 1100 \cong 10^3\right)$, and that the 10-bilayer LbL film might have 10 times more FePc than the 1-trilayer LbL film, the enhancement factor is estimated to be *ca.* 10^4.

The same estimation can be made for SERRS in relation to RRS. Considering the same band at 1450 cm^{-1} for the SERRS and RRS spectra in Fig. 3, the intensity ratio SERRS/RRS is given by $\left(\frac{62\,300}{4500} \cong 14\right)$. Besides, the RRS spectrum was collected with a laser power 10 times higher than the SERRS spectrum. Therefore, in this case, the enhancement factor is estimated to be *ca.* 140 ($\cong 10^2$). The higher enhancement factor found for SERS in relation to SERRS is in agreement with the model considering the electromagnetic mechanism.[70]

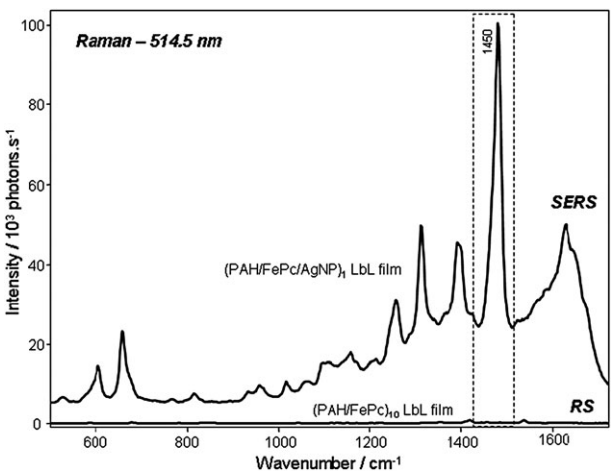

Fig. 4 Raman spectra recorded with the 514.5 nm laser line for LbL films containing 10 bilayers of PAH/FePc (RS) and 1 trilayer of PAH/FePc/AgNP (SERS).

As previously mentioned, this is just a rough estimation, especially if it is considered that in these LbL films both SERS and SERRS spectra have different profiles from spot to spot. However, in any case, the enhancement factors reported here are pretty reasonable considering those that we have reported for MPc's using the same estimation procedure. For instance, it was found enhancement factors around 10^4 for SERRS recorded for $PdPc_2$ PVD films,[34] at *ca.* 300 for SERRS collected for $YbPc_2$ LB films[37] and around 50 for SERRS recorded for RhPc LB films.[71] The SERS was not estimated for RhPc and $YbPc_2$ because the RS for the LB films on glass could not be detected even with long collecting times and several accumulations.

LbL film morphology—micro-Raman and SEM

The morphology of the LbL films was investigated at the micrometre scale through micro-Raman and SEM techniques. Fig. 5a presents the optical images for a LbL film containing 30 bilayers of PAH/FePc recorded with a digital camera (macroscale) and an optical microscopy (microscale, 50× magnification). The image with a digital camera shows a visually uniform film, with aggregates showing up at the micrometre scale. The optical image in Fig. 5b was recorded with an objective of 50× leading to a total magnification of 500× for a LbL film containing 10 bilayers of PAH/FePc. The image presents the same pattern of aggregates shown in the optical image in Fig. 5a. These aggregates are formed by FePc molecules according to the Raman data. For instance, Fig. 5c exhibits a line Raman mapping recorded with the 514.5 nm laser line (RS), which consists of 51 spectra collected point-by-point along a line of 50 μm with step of 1 μm. The change in the signal intensity along the line follows the aggregate spatial distribution whose spectra shown in Fig. 5d are characteristics of FePc in LbL films (both spectra were chosen among those 51 collected). Superposed to the optical image in Fig. 5b there is the mapped line whose brighter spots represent the more intense signals of the Raman band at 1519 cm^{-1}.

Fig. 5e shows a SEM image recorded with magnification of 5000× revealing details of the molecular aggregates, which have distinct sizes within micrometres. Similar SEM results were found by Bertoncello *et al.*[62] in LbL films containing bilayers of copper tetrasulfonated phthalocyanine (CuTsPc) structured as CuTsPc/CuTsPc. Fig. 5f brings a scheme relating both the morphology and the PAH-FePc chemical interactions when forming the LbL films. Since the pK_a of PAH is around 8.3,[72] both NH_2 and NH_3^+ groups are found at pH 5.5 used to grow the LbL films. Considering this fact and the ability of phthalocyanines to self-aggregate, the mechanism described here proposes that the FePc already aggregated in the chloroform solution interacts preferentially with the sites of PAH containing NH_2 groups leading to the formation of even larger aggregates on top of the PAH layer. Essential for the mechanism proposed are the FePc-PAH interaction, which was already inferred here in connection with the UV-Vis absorption and Raman scattering, and the presence of FePc aggregates in the chloroform solution confirmed by UV-Vis absorption.

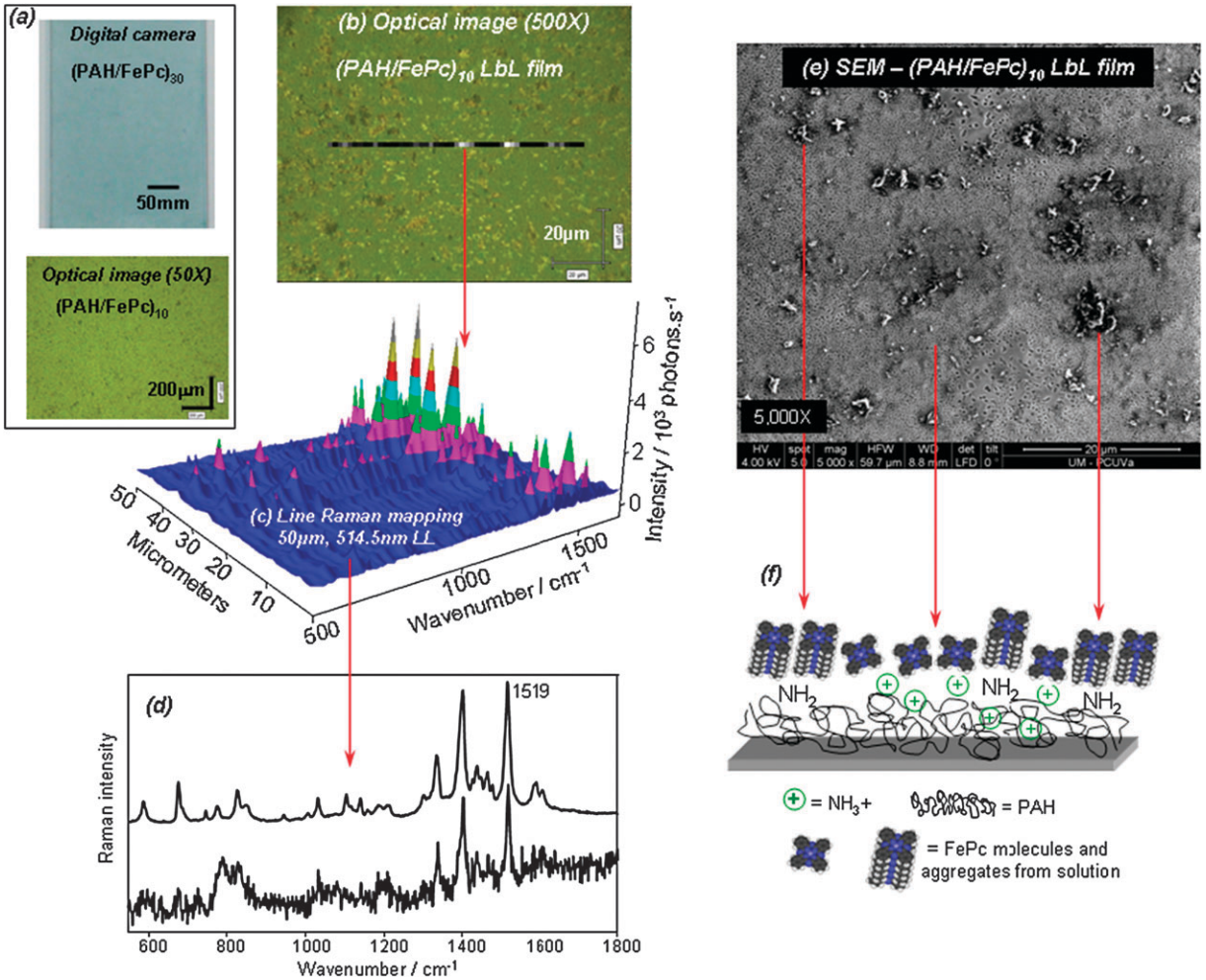

Fig. 5 (a) Optical images obtained using a digital camera for the LbL film containing 30 bilayers of PAH/FePc (top) and using an optical microscope (50× magnification) for the LbL film containing 10 bilayers of PAH/FePc (down). LbL film containing 10 bilayers of PAH/FePc: (b) optical image obtained using an optical microscope (500× magnification); (c) Raman line mapping built collecting spectra with the 514.5 nm laser line along a line of 50 µm with step of 1 µm exhibited in 3 dimensions (superposed to the optical image in 5b there is the mapped line whose brighter spots represent the more intense signals of the band at 1515 cm^{-1}); (d) Raman spectra chosen from the line mapping shown in 5c; (e) SEM image recorded with magnification of 5000×; (f) scheme representing the distribution of the FePc aggregates in the LbL films–the FePc aggregates in the chloroform solution are adsorbed onto PAH layers driven by the interaction with the NH_2 groups.

Concerning possible effects due to the incorporation of AgNPs, in terms of the FePc aggregates the morphology of the LbL films containing trilayers of PAH/FePc/AgNP is similar to that of PAH/FePc LbL films, which was expected since the interaction between FePc and AgNPs is mainly driven by physical adsorption. Therefore, the major difference is the presence of AgNPs as shown in the SEM images in Fig. 6a and b recorded with magnifications of 5000× and 50 000×, respectively. The AgNPs are adsorbed onto the FePc layer either as isolated or aggregates, which is consistent with the UV-Vis absorption data discussed in Fig. 2. It is found that the isolated AgNPs have a preferentially spherical-like shape with an average diameter at *ca.* 100 nm. Besides, the AgNPs can vary in size from 40 nm (isolated) until 300 nm (aggregated). The Fig. 6c shows a zoom of the SEM image present in Fig. 6b where isolated and aggregated AgNPs are seen in detail. Fig. 6d is a 3-dimensional view of the SEM image shown in Fig. 6b revealing the roughness of the surface of the LbL film covered by containing AgNPs.

LbL film molecular organization—FTIR spectroscopy

The phthalocyanine molecules are known to possess molecular organization when forming thin films.[15,16,24,66] In a recent work the molecular organization of FePc in PVD and LB films and FeTsPc in LbL films (aqueous media) was determined.[15] Here, the molecular organization investigation of FePc in the LbL film (non-aqueous medium) was carried out through FTIR spectroscopy. Fig. 7 displays the FTIR spectra for FePc in KBr pellet taken as reference and for LbL film of PAH/FePc with 12 bilayers deposited onto ZnSe and recorded in the transmission mode. The molecular organization is determined combining the FTIR data and the surface selection rules, which take into account basically two pieces of information:[66,73,74] (i) the intensity (*I*) of the

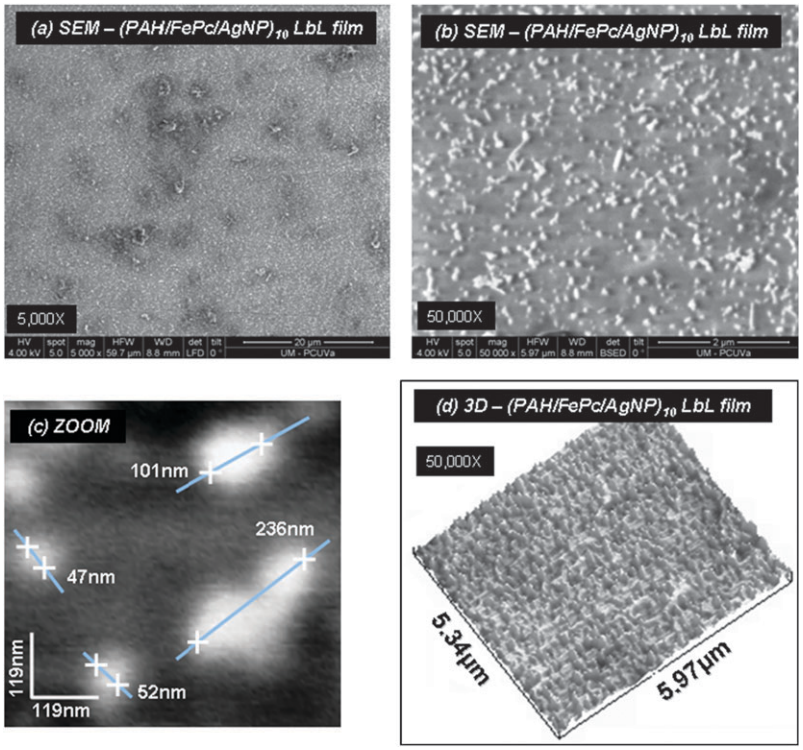

Fig. 6 SEM images recorded for LbL films containing 10 trilayers of PAH/FePc/AgNP with magnifications of (a) 5000× (scale = 20 μm) and (b) 50 000× (scale = 2 μm). (c) Zoom of the SEM image shown in (b); (d) 3-dimensional view of the SEM image shown in (b).

infrared absorption for a fixed molecule in the space depends on the scalar product between the electric field of the incident radiation ($\vec{E}$) and the transient dipole moment ($\vec{\mu}'$) of each vibrational mode of the molecule $\Rightarrow$ $I = \vec{E}\cdot\vec{\mu}'$; (ii) in the transmission mode the incident electric field is parallel to the substrate surface. The analysis is carried out considering some key bands, *i.e.*, those bands whose $\vec{\mu}'$ is parallel (in-plane) or perpendicular (out-of-plane) to the FePc macrocycle plane. The bands considered were at 729 cm^{-1} attributed to C–H wagging (out-of-plane), 751 cm^{-1} assigned to benzene deformation (in-plane), and 1117 and 1331 cm^{-1} that are attributed, respectively, to C–H bending (in-plane) and C=C or C=N stretching (pyrrole), which is also in the plane of the FePc macrocycle.[16,34,65,66]

The FTIR spectrum of the LbL film is seen to be dominated by the FePc normal modes whose $\vec{\mu}'$ is in the plane of the FePc macrocycle. Therefore, the FePc is preferentially placed with the macrocycle parallel to the substrate. This is confirmed by the great similarity between the FTIR spectra of LbL and LB[15] films. In the latter, it was found that the FePc are tilted between 0 and 45° in relation to the substrate. However, in the case of the LbL film, the band at 751 cm^{-1} assigned to benzene deformation (in-plane) is relatively more intense than that found for LB films, suggesting the tendency of the FePc to organize preferentially in a flat-on fashion. It is found in the literature for thin films of phthalocyanines that the molecular organization depends on both the preparation technique and metal in the center of the Pc ring. In the case of PVD films, experimental conditions such as deposition rate and substrate temperature play a key role.[34,66,75–77] For LB films there are fewer studies on molecular orientation, and it is known that transferring conditions such as surface pressure of deposition and dipper speed can be determinant.[78–81] In LbL films of PAH/FeTsPc prepared in aqueous media, distinct molecular organizations were found depending on the pH of the aqueous solutions. FeTsPc acquired a preferential flat-on orientation at pH 8.0[16] while it was randomly oriented at pH 5.5.[15]

Since the pH of the solutions used to fabricate the LbL films governs the electrostatic interactions, it is expected that the molecular organization in the film differs substantially with a change in pH.[82–84] However, in the case of PAH/FePc LbL film (prepared in non-aqueous medium), the interaction between the Fe and the pair of electrons of the NH_2 might play the main role on the FePc molecular organization. This is supported by two facts: (i) in non-aqueous media the electrostatic interactions can be discarded and (ii) the final molecular orientation coincides with the PAH/FeTsPc LbL film prepared at pH 8.0 where both electrostatic and Fe–NH_2 interactions were important.[16] Finally, FTIR results confirm the interaction between Fe and the NH_2 group. With regard to the Fe–NH_2 interaction, the FTIR spectra in Fig. 7 are consistent with the discussion based on SERRS and RRS in a previous section. For instance, in the PAH/FePc LbL film the FTIR bands related to the metal atom vibrations are suppressed or modified. The band at 1727 cm^{-1} assigned to the metal-axial ligand of FePc[16] is very strong in the FePc KBr pellet but it is vanished in the PAH/FePc LbL film. In addition, differences in the relative intensity appeared between the spectra for FePc powder and PAH/FePc LbL film in Fig. 7 for the following bands related to the Fe atom surroundings:[65,66] 718 cm^{-1} (isoindol deformation, N–Fe stretching), 751 cm^{-1} (benzene deformation, isoindol deformation, N–Fe stretching),

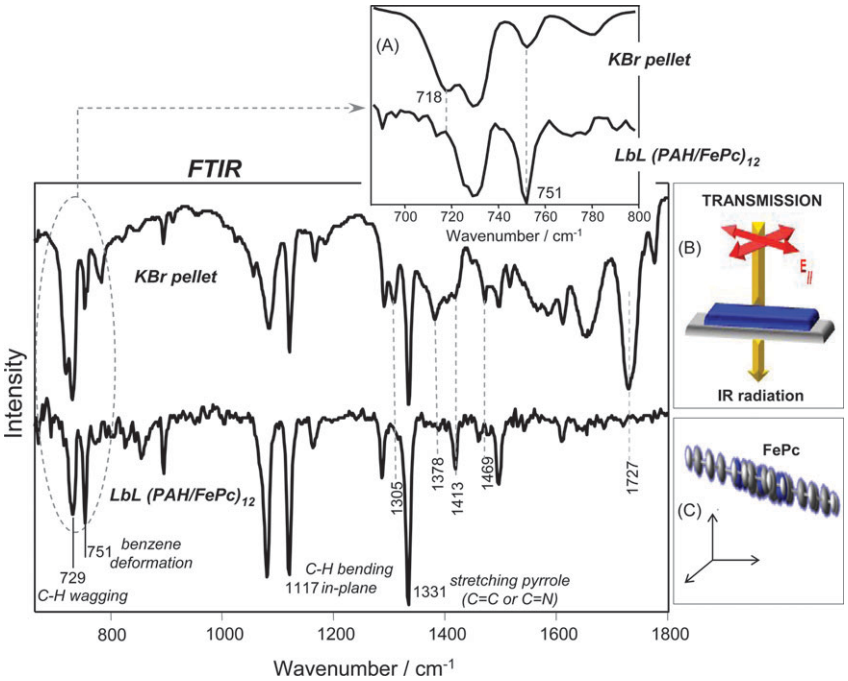

Fig. 7 FTIR spectra in the transmission mode for FePc in KBr pellet and PAH/FePc LbL film containing 12 bilayers. Insets: (A) zoom at the low wavenumber region; (B) illustration of the surface selection rules; (C) FePc molecular organization in the PAH/LbL film.

1305 cm^{-1} (N–Fe pyrrole C–N stretching, C–N C–H in-plane-bending), 1378 cm^{-1} (C–H pyrrole in-plane-bending, C–N_m C–C stretching), and 1413 cm^{-1} (C–H pyrrole in-plane-bending, C–N_m C–C stretching), where N_m is the macrocycle N atom (see Fig. 1).

LbL film electrochemical properties—cyclic voltammetry

In the last part of this work, the electrochemical and electrocatalytic properties of the LbL films were studied by cyclic voltammetry. Experiments were carried out in 0.1 M KCl aqueous solution from −1.0 to 1.0 V at a scan rate of 100 mV s^{-1}. Fig. 8a shows the voltammograms for LbL films deposited onto ITO containing 5 bilayers of PAH/FePc and 5 trilayers of PAH/FePc/AgNP. The cyclic voltammogram of a film consisting of 5 bilayers of PAH/FeTsPc (prepared from aqueous solution) was also included in the study for comparison. As observed in Fig. 8a, ITO electrodes modified with LbL films show an irreversible cathodic peak at −0.7 V whose intensity follows the sequence ITO < PAH/FeTsPc < PAH/FePc < PAH/FePc/AgNP. This trend might be directly related to the amount of phthalocyanine adsorbed onto the ITO. The latter was observed by UV-Vis absorption spectroscopy (Figure not shown for PAH/FeTsPc). Besides, considering the assignment of the peak at −0.7 V, according to Chaves *et al.*[85] this peak was observed for FeTcPc (iron tetracarboxylated phthalocyanine) at pH 6 and it was associated with the reduction process involving the macrocycle ring of Pc. Corio *et al.*[69] working with spectroelectrochemical (SERS) for FePc have also assigned this peak to the Pc macrocycle ring reduction; however due to the delocalization of the π electrons of the Pc ring, a partial reduction of the Fe(II) central ion was not discarded by them.

The electrochemical catalytic effect of the LbL films was tested towards dopamine. Fig. 8b shows the voltammograms recorded using the ITO-modified electrode with the LbL film containing 5 bilayers of PAH/FePc immersed in solutions with different concentrations of dopamine (from 2.0×10^{-6} M up to 2.75×10^{-4} M). The curves are dominated by an anodic peak with maximum at *ca.* 0.12 V associated with the dopamine oxidation. The intensity of the peak associated with dopamine is higher when using LbL films of PAH/FePc and of PAH/FePc/AgNP deposited in a non-aqueous medium. This is consistent with the better electrocathalytic activity shown by the unsubstituted phthalocyanine. The electrocatalytic effect is improved in the presence of AgNPs.

Fig. 8c shows the linear relationship ($r^2 = 0.983$) between the peak current and the dopamine concentration in the range between 2.0×10^{-6} M and 9.7×10^{-5} M. The detection limit calculated from IUPAC (3σ criteria) was 0.86×10^{-6} M. The limit of detection and quantification were calculated statistically as follows: LD = $k \times$ SB/b, where SB is the standard deviation of the blank, b is the sensitivity of the method (determined as the slope of the calibration curve) and k is a statistical constant (a value of 3 for LD is widely accepted)[86] that is consistent with the reported value for LbL films of phthalocyanines.[87]

The intensity of the peak associated with the oxidation of dopamine depends on the chemical nature of the LbL film deposited onto the ITO electrode as shown in Fig. 8d. Films formed by 5 bilayers of PAH/FePc produce a response similar to that observed in films formed by 5 trilayers of PAH/FePc/AgNP. The only difference lies in the sharp peak due to the AgNPs at 0.16 V. The oxidation current of the anodic peak potential associated with dopamine is higher when using the film containing 5 bilayers of PAH/FePc than for ITO glass and

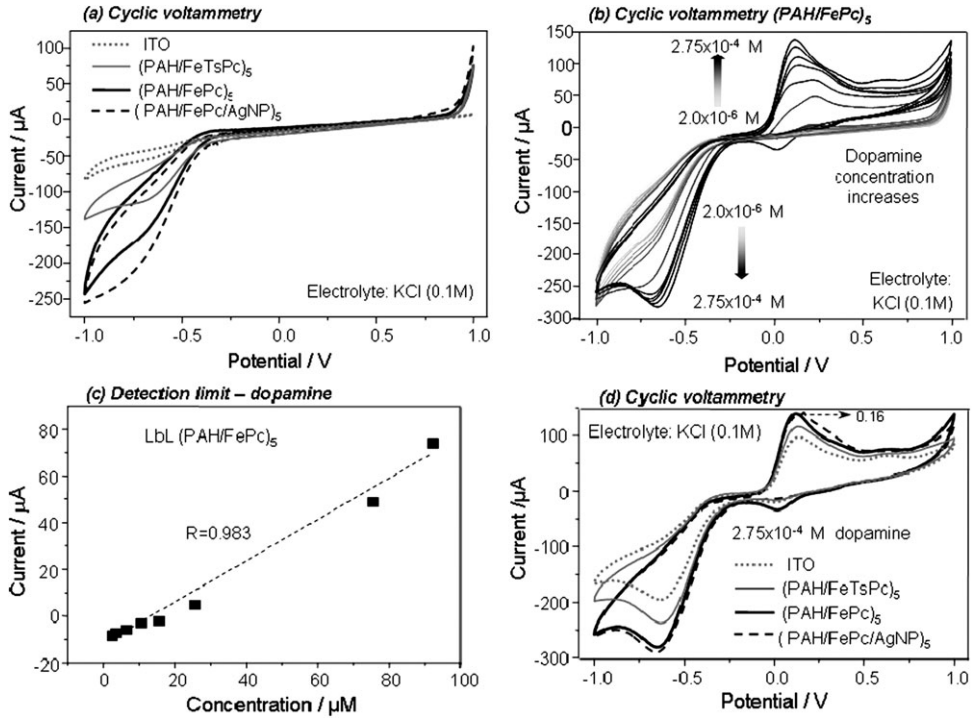

Fig. 8 Cyclic voltammograms recorded with 100 mV s^{-1} in 0.1 M KCl for (a) ITO and LbL films of $(PAH/FeTsPc)_5$, $(PAH/FePc)_5$ and $(PAH/FePc/AgNP)_5$; (b) LbL film of $(PAH/FePc)_5$ in the presence of dopamine with concentrations from 2.0×10^{-6} up to 2.75×10^{-4} M; (c) anodic current peak *vs*. dopamine molar concentration; (d) ITO and LbL films of $(PAH/FeTsPc)_5$, $(PAH/FePc)_5$ and $(PAH/FePc/AgNP)_5$ in the presence of dopamine at 2.75×10^{-4} M.

LbL film prepared from PAH/FeTsPc aqueous solution. This result is of particular interest because previous work[16] has demonstrated that the LbL film of PAH/FeTsPc grown in aqueous media and tested in acetonitrile solutions does not show a response towards dopamine. This lack of response has been attributed to the occurrence of Fe–NH_2 interactions in the film, which may hinder the interaction between dopamine and Fe atoms. In our case, the cyclic voltammograms were carried out in water and such a hindering effect was not observed either in PAH/FePc or in PAH/FeTsPc films. Besides, using water as electrolytic media, the improved catalytic effect of the PAH/FePc films–when compared with PAH/FeTsPc films–might be explained by the presence of FePc aggregates as described in Fig. 5f. The macrocycles approach each other through π–π interactions forming the aggregates, which means that not all the FePc molecules are interacting with PAH, consistent with the SERRS data discussed in Fig. 3. Therefore, there are FePc molecules whose Fe atoms can coordinate with dopamine molecules. In addition, the LbL films of PAH/FeTsPc used in ref. 16 were fabricated in an aqueous medium at pH 8.0. Under these conditions aggregation is minimized as supported by the reported UV-Vis absorption spectra, reinforcing our hypothesis of the role played by FePc aggregates in the electroactivity of PAH/FePc LbL films despite the Fe–NH_2 interactions.

Conclusion

The LbL technique was successfully applied to produce thin films using FePc in non-aqueous media either as bilayers of $(PAH/FePc)_n$ or as trilayers of $(PAH/FePc/AgNP)_n$. The morphology revealed the presence of FePc aggregates in the LbL film, which were previously formed in the FePc chloroform solution. Although the presence of aggregates at the micrometre scale may suggest a lack of control in the fabrication of the PAH/FePc layers, the linear growth evidenced by UV-Vis absorption data and the FTIR and cyclic voltammetry results demonstrate that the properties are well defined on average, leading to reproducible results. In terms of molecular organization, the FePc are found to be preferentially placed with the Pc ring parallel to the substrate (flat-on). Furthermore, the AgNPs are found to physically adsorb onto the FePc layers as isolates or aggregates, thus allowing one to obtain both SERS and SERRS spectra. The effectiveness of achieving the surface-enhanced phenomenon is demonstrated by enhancement factors of *ca.* 10^4 for SERS and 10^2 for SERRS. The LbL films with bi- and trilayers were effectively applied as a proof-of-principle in the detection of dopamine in KCl aqueous solutions down to 6×10^{-6} M using cyclic voltammetry. It is also revealed that the electroactivity of FePc is maintained in the presence of dopamine despite the Fe–NH_2 interaction, for which the FePc aggregates might play a key role. The films deposited in non-aqueous medium display an increased sensitivity towards dopamine and justify their use as catalysts and electrochemical sensors. The micro-Raman and the FTIR data revealed that the interaction between Fe and NH_2 groups of PAH is the main driving force for the growth of the LbL films with FePc in non-aqueous media. This finding is supported by a theoretical study of Tran and Kummel[88]

who suggested a chemical adsorption of NH_3 onto FePc films through the Fe atoms.

Acknowledgements

We acknowledge FAPESP and CAPES (process 118/06) from Brazil and MICINN (PHB2005-0057-PC) from Spain for the financial support.

References

1 R. K. Iler, *J. Colloid Interface Sci.*, 1966, **21**, 569–594.
2 L. Netzer and J. Sagiv, *J. Am. Chem. Soc.*, 1983, **105**, 674–676.
3 G. Decher, J. D. Hong and J. Schmitt, *Thin Solid Films*, 1992, **210–211**, 831–835.
4 M. Ferreira, J. H. Cheung and M. F. Rubner, *Thin Solid Films*, 1994, **244**, 806–809.
5 J. H. Cheung, A. F. Fou and M. F. Rubner, *Thin Solid Films*, 1994, **244**, 985–989.
6 L. Zhang, Y. H. Shen, A. J. Xie, S. K. Li and Y. M. Li, *J. Mater. Chem.*, 2009, **19**, 1884–1893.
7 L. G. Paterno, M. A. G. Soler, F. J. Fonseca, J. P. Sinnecker, E. H. C. P. Sinnecker, E. C. D. Lima, M. A. Novak and P. C. Morais, *J. Phys. Chem. C*, 2009, **113**, 5087–5095.
8 F. Kurniawan, V. Tsakova and V. M. Mirsky, *J. Nanosci. Nanotechnol.*, 2009, **9**, 2407–2412.
9 P. H. B. Aoki, D. Volpati, A. Riul Jr., W. Caetano and C. J. L. Constantino, *Langmuir*, 2009, **25**, 2331–2338.
10 M. L. Moraes, M. S. Baptista, R. Itri, V. Zucolotto and O. N. Oliveira Jr, *Mater. Sci. Eng., C*, 2008, **28**, 467–471.
11 X. Y. Li, P. W. Fan, X. L. Tuo, Y. N. He and X. G. Wang, *Thin Solid Films*, 2009, **517**, 2055–2062.
12 G. C. Zhang and M. H. Liu, *J. Mater. Chem.*, 2009, **19**, 1471–1476.
13 J. R. Siqueira, M. H. Abouzar, M. Backer, V. Zucolotto, A. Poghossian, O. N. Oliveira Jr. and M. J. Schoning, *Phys. Status Solidi A*, 2009, **206**, 462–467.
14 C. Y. He, W. B. Duan, G. Shi, Y. Q. Wu, Q. Y. Ouyang and Y. L. Song, *Appl. Surf. Sci.*, 2009, **255**, 4696–4701.
15 D. Volpati, P. Alessio, A. A. Zanfolim, F. C. Storti, A. E. Job, M. Ferreira, A. Riul Jr., O. N. Oliveira Jr. and C. J. L. Constantino, *J. Phys. Chem. B*, 2008, **112**, 15275–15282.
16 V. Zucolotto, M. Ferreira, M. R. Cordeiro, C. J. L. Constantino, D. T. Balogh, A. R. Zanatta, W. C. Moreira and O. N. Oliveira Jr., *J. Phys. Chem. B*, 2003, **107**, 3733–3737.
17 W. S. Alencar, F. N. Crespilho, M. R. M. C. Santos, V. Zucolotto, O. N. Oliveira Jr. and W. C. Silva, *J. Phys. Chem. C*, 2007, **111**, 12817–12821.
18 J. R. Siqueira, F. N. Crespilho, V. Zucolotto and O. N. Oliveira Jr., *Electrochem. Commun.*, 2007, **9**, 2676–2680.
19 H. Benten, N. Kudo, H. Ohkita and S. Ito, *Thin Solid Films*, 2009, **517**, 2016–2022.
20 Y. N. Jin, L. Xu, L. D. Zhu, W. J. An and G. G. Gao, *Thin Solid Films*, 2007, **515**, 5490–5497.
21 W. J. Doherty, R. Friedlein and W. R. Salaneck, *J. Phys. Chem. C*, 2007, **111**, 2724–2729.
22 C. Y. He, Y. Q. Wu, G. Shi, L. Jiang, W. Duan, Y. Song and Q. Chang, *J. Porphyrins Phthalocyanines*, 2007, **11**, 496–502.
23 Y. Yang, L. Xu, B. Xu, X. Du and W. Guo, *Mater. Lett.*, 2009, **63**, 608–610.
24 C. C. Leznoff and A. B. P. Lever, *Phthalocyanines: Properties and Applications*, VCH Publishers, 1989, vol. 1–3.
25 M. L. Rodriguez-Mendez, V. Parra, C. Apetrei, S. Villanueva, M. Gay, N. Prieto, J. Martinez and J. A. de Saja, *Microchim. Acta*, 2008, **163**, 23–31.
26 X. Cai, Y. X. Zhang, D. D. Qi and J. Z. Jiang, *J. Phys. Chem. A*, 2009, **113**, 2500–2506.
27 L. F. Santos, R. M. Faria, T. Del Cano, J. A. de Saja, C. J. L. Constantino, C. A. Amorim and S. Mergulhao, *J. Phys. D*, 2008, **41**, 125107.
28 M. R. Ke, J. D. Huang and S. M. Weng, *J. Photochem. Photobiol., A*, 2009, **201**, 23–31.
29 R. J. Mortimer, A. L. Dyer and J. R. Reynolds, *Displays*, 2006, **27**, 2–18.
30 N. Peltekis, B. N. Holland, S. Krishnamurthy, I. T. McGovern, N. R. J. Poolton, S. Patel and C. McGuinness, *J. Am. Chem. Soc.*, 2008, **130**, 13008–13012.
31 L. De Boni, E. Piovesan, L. Gaffo and C. R. Mendonca, *J. Phys. Chem. A*, 2008, **112**, 6803–6807.
32 T. Choi and T. D. Milster, *Opt. Eng.*, 2006, **45**, 064302.
33 K. C. Chiu, L. T. Juey, C. F. Su, S. J. Tang, M. N. Jong, S. S. Wang, J. S. Wang, C. S. Yang and W. C. Chou, *J. Cryst. Growth*, 2008, **310**, 1734–1738.
34 L. Gaffo, C. J. L. Constantino, W. C. Moreira, R. F. Aroca and O. N. Oliveira Jr., *J. Raman Spectrosc.*, 2002, **33**, 833–837.
35 S. Karan and B. Mallik, *Nanotechnology*, 2008, **19**, 495202.
36 Z. M. Wei, W. Xu, W. P. Hu and D. B. Zhu, *Langmuir*, 2009, **25**, 3349–3351.
37 L. Gaffo, C. J. L. Constantino, W. C. Moreira, R. F. Aroca and O. N. Oliveira Jr., *Langmuir*, 2002, **18**, 3561–3566.
38 C. Boeckler, A. Feldhoff and T. Oekermann, *Adv. Funct. Mater.*, 2007, **17**, 3864–3869.
39 K. Kaunisto, H. Vahasalo, V. Chukharev, N. V. Tkachenko, P. Vivo, M. Niemi, A. Tolkki, A. Efimov and H. Lemmetyinen, *Thin Solid Films*, 2009, **517**, 2988–2993.
40 X. Mo, H. Z. Chen, Y. Wang, M. M. Shi and M. Wang, *J. Phys. Chem. B*, 2005, **109**, 7659–7663.
41 Y. H. Cheng, K. Y. Lin and M. C. M. Lee, *Thin Solid Films*, 2009, **517**, 2959–2962.
42 R. B. Ye, M. Baba, K. Suzuki and K. Mori, *Thin Solid Films*, 2009, **517**, 3001–3004.
43 D. Atilla, N. Kilinc, F. Yuksel, A. G. Gurek, Z. Z. Ozturk and V. Ahsen, *Synth. Met.*, 2009, **159**, 13–21.
44 Y. J. Feng and N. Alonso-Vante, *Phys. Status Solidi B*, 2008, **245**, 1792–1806.
45 F. I. Bohrer, C. N. Colesniuc, J. Park, M. E. Ruidiaz, I. K. Schuller, A. C. Kummel and W. C. Trogler, *J. Am. Chem. Soc.*, 2009, **131**, 478–485.
46 J. A. De Saja and M. L. Rodriguez-Mendez, *Adv. Colloid Interface Sci.*, 2005, **116**, 1–11.
47 P. C. Lee and D. Meisel, *J. Phys. Chem.*, 1982, **86**, 3391–3395.
48 R. A. Alvarez-Puebla, E. Arceo, P. J. G. Goulet, J. J. Garrido and R. F. Aroca, *J. Phys. Chem. B*, 2005, **109**, 3787–3792.
49 K. Kneipp and D. Fassler, *Chem. Phys. Lett.*, 1984, **106**, 498–502.
50 P. Hildebrandt and M. Stockburger, *J. Phys. Chem.*, 1984, **88**, 5935–5944.
51 Y. Wang, S. K. Eswaramoorthy, L. J. Sherry, J. A. Dieringer, J. P. Camden, G. C. Schatz, R. P. Van Duyne and L. D. Marks, *Ultramicroscopy*, 2009, **109**, 1110–1113.
52 A. Šileikaitė, J. Puišo, I. Prosyčevas and S. Tamulevičius, *Mater. Sci.*, 2009, **15**, 21–27.
53 M. Moskovits, *Rev. Mod. Phys.*, 1985, **57**, 783–826.
54 C. J. L. Constantino and R. F. Aroca, *J. Raman Spectrosc.*, 2000, **31**, 887–890.
55 P. J. G. Goulet, D. S. Dos Santos Jr., R. A. Alvarez-Puebla, O. N. Oliveira Jr. and R. F. Aroca, *Langmuir*, 2005, **21**, 5576–5581.
56 P. H. B. Aoki, P. Alessio, J. A. De Saja Saez and C. J. L. Constantino, *J. Raman Spectrosc.*, 2010, **41**, 40.
57 N. P. W. Pieczonka, P. J. G. Goulet and R. F. Aroca, *J. Am. Chem. Soc.*, 2006, **128**, 12626–12627.
58 J. J. Laserna, *Modern Techniques in Raman Spectroscopy*, John Wiley & Sons, Toronto, 1996.
59 P. J. Camp, A. C. Jones, R. K. Neely and N. M. Speirs, *J. Phys. Chem. A*, 2002, **106**, 10725–10732.
60 V. I. Vlaskin, O. P. Dimitriev, Z. I. Kazantseva and A. V. Nabok, *Thin Solid Films*, 1996, **286**, 40–44.
61 P. D. Fuqua and B. Dunn, *J. Sol-Gel Sci. Technol.*, 1998, **11**, 241–250.
62 P. Bertoncello and M. Peruffo, *Colloids Surf., A*, 2008, **321**, 106–112.
63 K. Kasuga and M. Tsutsui, *Coord. Chem. Rev.*, 1980, **32**, 67–95.
64 C. Woojung, M. Naito, R. Fujii, M. Morisue and M. Fujiki, *Thin Solid Films*, 2009, **518**, 625–628.
65 Z. Liu, X. Zhang, Y. Zhang and J. Jiang, *Spectrochim. Acta, Part A*, 2007, **67**, 1232–1246.
66 R. Aroca and A. Thedchanamoorthy, *Chem. Mater.*, 1995, **7**, 69–74.

67 G. J. Kovacs, R. O. Loutfy, P. S. Vincett, C. Jennings and R. F. Aroca, *Langmuir*, 1986, **2**, 689–694.
68 C. J. L. Constantino, J. Duff and R. Aroca, *Spectrochim. Acta, Part A*, 2001, **57**, 1249–1259.
69 P. Corio, J. C. Rubim and R. Aroca, *Langmuir*, 1998, **14**, 4162–4168.
70 P. J. Tarcha, J. De Saja-Gonzalez, S. Rodriguez-Llorente and R. F. Aroca, *Appl. Spectrosc.*, 1999, **53**, 43–48.
71 L. Gaffo, C. J. L. Constantino, W. C. Moreira, R. F. Aroca and O. N. Oliveira, *Spectrochim. Acta, Part A*, 2004, **60**, 321–327.
72 J. Choi and M. F. Rubner, *Macromolecules*, 2005, **38**, 116–124.
73 M. K. Debe, *Prog. Surf. Sci.*, 1987, **24**, 1–282.
74 P. A. Antunes, C. J. L. Constantino, R. Aroca and J. Duff, *Appl. Spectrosc.*, 2001, **55**, 1341–1346.
75 M. Brinkmann, J.-C. Wittmann, M. Barthel, M. Hanack and C. Chaumont, *Chem. Mater.*, 2002, **14**, 904–914.
76 K. Sugiyama, S. Iizuka, H. Yashir, H. Fukuda and Y. Shimoyama, *Jpn. J. Appl. Phys.*, 2008, **47**, 492–495.
77 T. Del Caño, V. Parra, M. L. Rodríguez-Méndez, R. F. Aroca and De Saja, *Appl. Surf. Sci.*, 2005, **246**, 327–333.
78 M. Rikukawa and M. F. Rubner, *Langmuir*, 1994, **10**, 519–524.
79 Y. Gorbunova, M. L. Rodriguez-Mendez, I. P. Kalashnikova, L. G. Tomilova and J. A. de Saja, *Langmuir*, 2001, **17**, 5004–5010.
80 L. Gaffo, A. W. Rinaldi, M. J. L. Santos and E. M. Girotto, *J. Porphyrins Phthalocyanines*, 2007, **11**, 618–622.
81 N. Kumaran, C. L. Donley, S. B. Mendes and N. R. Armstrong, *J. Phys. Chem. C*, 2008, **112**, 4971–4977.
82 F. N. Crespilho, V. Zucolotto Jr., C. J. L. Constantino, F. C. Nart and O. N. Oliveira Jr., *Environ. Sci. Technol.*, 2005, **39**, 5385–5389.
83 V. Zucolotto, M. Ferreira, M. R. Cordeiro, C. J. L. Constantino, W. C. Moreira and O. N. Oliveira Jr., *Sens. Actuators, B*, 2006, **113**, 809–815.
84 L. Liu, X. Jin, S. Yang, Z. Chen and X. Lin, *Biosens. Bioelectron.*, 2007, **22**, 3210–3216.
85 J. A. P. Chaves, M. F. A. Araújo, J. de. J. G. Varela Júnior and A. A. Tanaka, *Ecletica Quim.*, 2003, **28**, 9–19.
86 J. C. Miller and J. N. Miller, *Estadistica para Quimica Analitica*, Addison-Wesley Iberoamericana, Wilmington, Delaware, 1993.
87 M. F. Zampa, A. C. F. de Brito, I. L. Kitagawa, C. J. L. Constantino, O. N. Oliveira Jr., H. N. da Cunha, V. Zucolotto, J. R. dos Santos Jr. and C. Eiras, *Biomacromolecules*, 2007, **8**, 3408–3413.
88 N. L. Tran and A. C. Kummel, *J. Chem. Phys.*, 2007, **127**, 214701.